Cystatin B-deficiency triggers ectopic histone H3 tail cleavage during neurogenesis

Daura, Eduard

2021-08

Daura , E , Tegelberg , S , Yoshihara , M , Jackson , C , Simonetti , F , Aksentjeff , K , Ezer , S , Hakala , P , Katayama , S , Kere , J , Lehesjoki , A-E & Joensuu , T 2021 , ' Cystatin B-deficiency triggers ectopic histone H3 tail cleavage during neurogenesis ' , Neurobiology of Disease , vol. 156 , 105418 . https://doi.org/10.1016/j.nbd.2021.105418

http://hdl.handle.net/10138/339880
https://doi.org/10.1016/j.nbd.2021.105418

Neurobiology of Disease 156 (2021) 105418

Contents lists available at ScienceDirect

Neurobiology of Disease

journal homepage: www.elsevier.com/locate/ynbdi

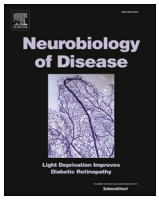

Cystatin B-deficiency triggers ectopic histone H3 tail cleavage during neurogenesis

Eduard Daura [a,b], Saara Tegelberg [a,b], Masahito Yoshihara [c], Christopher Jackson [d,e], Francesca Simonetti [a,b], Katri Aksentjeff [a,b], Sini Ezer [a,b], Paula Hakala [a,b], Shintaro Katayama [a,b,c], Juha Kere [a,c,e], Anna-Elina Lehesjoki [a,b,*,1], Tarja Joensuu [a,b,1]

[a] Folkhälsan Research Center, 00290 Helsinki, Finland
[b] Medicum, Faculty of Medicine, University of Helsinki, 00290 Helsinki, Finland
[c] Department of Biosciences and Nutrition, Karolinska Institutet, 141 83 Stockholm, Sweden
[d] Department of Biochemistry and Developmental Biology, Faculty of Medicine, University of Helsinki, 00290 Helsinki, Finland
[e] Stem Cells and Metabolism Research Program, Faculty of Medicine, University of Helsinki, 00290 Helsinki, Finland

ARTICLE INFO

Keywords:
Cystatin B
Histone clipping
Histone cleavage
Cathepsin
Neural differentiation
Progressive myoclonus epilepsy

ABSTRACT

Cystatin B (CSTB) acts as an inhibitor of cysteine proteases of the cathepsin family and loss-of-function mutations result in human brain diseases with a genotype-phenotype correlation. In the most severe case, CSTB-deficiency disrupts brain development, and yet the molecular basis of this mechanism is missing. Here, we establish CSTB as a regulator of chromatin structure during neural stem cell renewal and differentiation. Murine neural precursor cells (NPCs) undergo transient proteolytic cleavage of the N-terminal histone H3 tail by cathepsins B and L upon induction of differentiation into neurons and glia. In contrast, CSTB-deficiency triggers premature H3 tail cleavage in undifferentiated self-renewing NPCs and sustained H3 tail proteolysis in differentiating neural cells. This leads to significant transcriptional changes in NPCs, particularly of nuclear-encoded mitochondrial genes. In turn, these transcriptional alterations impair the enhanced mitochondrial respiration that is induced upon neural stem cell differentiation. Collectively, our findings reveal the basis of epigenetic regulation in the molecular pathogenesis of CSTB deficiency.

1. Introduction

Cystatin B (CSTB) is a ubiquitously expressed potent reversible and competitive inhibitor of cysteine proteases of the cathepsin family (Rawlings and Barrett, 1990; Turk and Bode, 1991). CSTB localizes mainly to the nucleus of immature proliferating cells (Alakurtti et al., 2005; Brännvall et al., 2003; Riccio et al., 2001). In differentiated cells, it is also found in the cytoplasm where it is associated with a subset of lysosomes. CSTB function has been associated with biological processes such as apoptosis (Pennacchio et al., 1998), oxidative stress response (Lehtinen et al., 2009), cell cycle regulation (Ceru et al., 2010), inflammation (Maher et al., 2014), synapse physiology (Gorski et al., 2020; Penna et al., 2019) and neurogenesis (Di Matteo et al., 2020). However, the molecular mechanisms by which CSTB mediates these effects remain largely unknown.

Biallelic loss-of-function mutations in the *CSTB* gene underlie human neurological diseases. The severity of these disorders correlates with the degree of residual CSTB expression. Partial loss of CSTB function leads to progressive myoclonus epilepsy, EPM1 (OMIM 254800), a neurodegenerative disease with onset between 6 and 15 years of age (Lehesjoki and Kalviainen, 1993; Pennacchio et al., 1996). In contrast, a total loss of function causes a neonatal-onset encephalopathy (Mancini et al., 2016; O'Brien et al., 2017). EPM1 is characterized by progressive drug-resistant myoclonus, epilepsy and ataxia, with cognition being largely preserved (Lehesjoki and Kalviainen, 1993). EPM1 is most commonly caused by homozygosity for a dodecamer repeat expansion mutation in the promoter region of *CSTB,* resulting in a 90–95% decrease in *CSTB* mRNA expression (Joensuu et al., 2007; Lalioti et al., 1997). Individuals compound heterozygous for the repeat expansion and a null mutation develop a more severe form of EPM1, with an earlier age of onset, more severe myoclonus and poorer cognitive performance (Canafoglia et al., 2012; Koskenkorva et al., 2011). The neonatal-onset encephalopathy is

* Corresponding author at: Folkhälsan Research Center, 00290 Helsinki, Finland.
E-mail address: anna-elina.lehesjoki@helsinki.fi (A.-E. Lehesjoki).
[1] These authors contributed equally to this work.

https://doi.org/10.1016/j.nbd.2021.105418
Received 29 January 2021; Received in revised form 30 April 2021; Accepted 4 June 2021
Available online 5 June 2021

caused by biallelic null mutations of *CSTB*, and manifests as severe developmental delay, progressive microcephaly, and hypomyelination on brain imaging (Mancini et al., 2016; O'Brien et al., 2017).

A *Cstb*-knockout ($Cstb^{-/-}$) mouse model recapitulates key features of EPM1, including the myoclonus, ataxia and progressive brain degeneration (Buzzi et al., 2012; Manninen et al., 2013; Manninen et al., 2014; Pennacchio et al., 1998; Shannon et al., 2002; Tegelberg et al., 2012). We previously demonstrated that early gliosis with consequent inflammation in the $Cstb^{-/-}$ mouse brain precedes the onset of myoclonus and neurodegeneration (Okuneva et al., 2015; Tegelberg et al., 2012). $Cstb^{-/-}$ mice also show altered GABAergic signaling in the cerebella prior to glial activation, which coincides with the development of GABAergic synapses (Joensuu et al., 2014). In line with these findings, CSTB function is required for appropriate interneuron migration in the

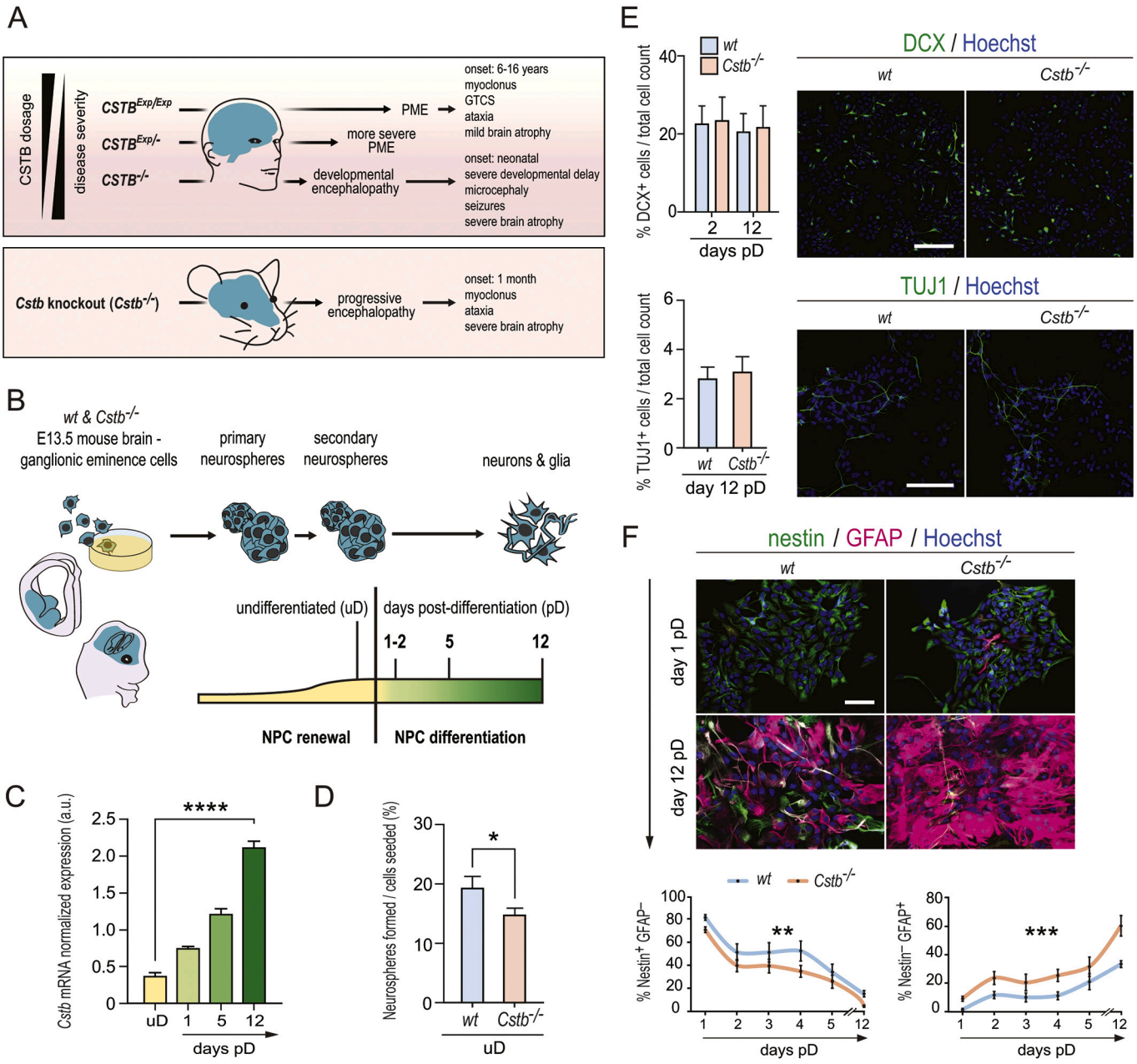

Fig. 1. A cultured cell model of neural stem cell renewal and differentiation to study CSTB function. A: Phenotypes associated with biallelic loss of CSTB function in human and in mice. $CSTB^{Exp/Exp}$: homozygosity for the dodecamer repeat expansion mutation; $CSTB^{Exp/-}$: compound heterozygosity for the expansion and null mutations; $CSTB^{-/-}$: biallelic null mutations; PME: progressive myoclonus epilepsy; GTCS: generalized tonic-clonic seizures. B: Schematic representation of the experimental model used in this study. C: RT-qPCR analysis of *Cstb* mRNA expression in self-renewing and differentiating *wt* NPCs. $Cstb^{-/-}$ uD NPCs were used as a negative control. The chart depicts *Cstb* expression normalized to mRNA level of *Rpl19* ± SEM ($n = 5$, $F_{(4,16)} = 182.9$, $p < 0.0001$, One-way ANOVA). The results were posteriorly validated by normalization to mRNA levels of *Atp5c1* and *Ywhaz* ($n = 5$). D: A chart depicting the average proportion of *wt* and $Cstb^{-/-}$ NPCs which gave rise to a secondary neurosphere following 8 days in culture ± SEM ($n = 6$, $t_{(10)} = 2.244$, $p = 0.048$, *t*-test). E: Representative immunofluorescence images of differentiating *wt* and $Cstb^{-/-}$ NPCs stained for doublecortin (DCX), class III β tubulin (TUJ1) and DNA (Hoechst). Scale bar = 50 μm. The charts depict the proportion of DCX-positive cells at days 2 and 12 pD and of TUJ1-positive cells at day 12 pD over total cell count as average ± SEM ($n = 5$). F: Representative immunofluorescence image of differentiating *wt* and $Cstb^{-/-}$ NPCs stained for nestin, GFAP and DNA (Hoechst). Scale bar = 50 μm. The charts depict the proportion of nestin-positive GFAP-negative cells and nestin-negative GFAP-positive cells over total cell count at six time-points pD ± SEM ($n = 8$, $nestin^+$ $GFAP^-$: Chisq = 9.261, $p = 0.002$, linear mixed model; $nestin^-$ $GFAP^+$: Chisq = 16.688, $p = 4.405E\text{-}05$, linear mixed model).

embryonic mouse brain (Di Matteo et al., 2020). At the early symptomatic stages, the number of GABAergic presynaptic terminals and ligand binding to $GABA_A$ receptors are reduced in *Cstb*$^{-/-}$ mouse cerebella with no alterations in the number of cerebellar interneurons (Joensuu et al., 2014). In older mice, CSTB deficiency leads to a progressive loss of inhibitory interneurons and decreased GABAergic inhibition in the cortex (Buzzi et al., 2012). Taken together, the data suggest CSTB-deficiency affects the development, maturation and integrity of inhibitory neuronal networks.

CSTB inhibits cathepsin L (Ceru et al., 2010; Turk and Bode, 1991), a cysteine protease known to regulate cell cycle progression through proteolytic processing of the CDP/Cux transcription factor, stabilization of epigenetic heterochromatin marks and sperm histone degradation (Adams-Cioaba et al., 2011; Bulynko et al., 2006; Duncan et al., 2008; Goulet et al., 2004; Morin et al., 2012). Moreover, cathepsin L is one of several intracellular proteases that have emerged as epigenetic regulators by cleavage of histone tails, particularly during cell-state transitions (Duncan et al., 2008; Khalkhali-Ellis et al., 2014; Kim et al., 2016). Proteolytic processing of histone tails is an evolutionarily conserved mechanism that impacts chromatin structure on multiple levels. On the one hand, it may lead to simultaneous removal of multiple histone post-translational modifications, an effect that can only be reversed through histone turnover (Allis et al., 1980; Duncan et al., 2008; Santos-Rosa et al., 2009). While on the other, the proteolytic removal of histone tails may lead to a more open nucleosome conformation, reducing intra-nucleosomal interactions and increasing DNA accessibility (Andresen et al., 2013; Iwasaki et al., 2018; Nurse et al., 2013). Histone cleavage has been implicated in transcriptional regulation in several organs and organisms (Azad et al., 2018; Duarte et al., 2014; Herrera-Solorio et al., 2019; Kim et al., 2016; Melo et al., 2017; Santos-Rosa et al., 2009). However, the upstream regulation and downstream effects of this mechanism remain poorly defined (Yi and Kim, 2018).

The genotype-phenotype correlations in patients with biallelic *CSTB* mutations and the phenotype of *Cstb*$^{-/-}$ mice imply a pivotal role for CSTB in brain development and maintaining neuronal integrity upon brain maturation. Since CSTB functions as an endogenous inhibitor of cathepsin L, we investigated the hypothesis that CSTB participates in chromatin remodeling during brain development. We found that CSTB regulates histone H3 tail proteolytic cleavage during neural stem cell differentiation through the inhibition of cysteine cathepsins B and L. The absence of CSTB results in premature H3 cleavage in undifferentiated and sustained H3 proteolysis in differentiating NPCs, leading to altered expression of nuclear-encoded mitochondrial genes and impaired mitochondrial respiratory function.

2. Results

2.1. Modelling neural stem cell renewal and differentiation in the absence of CSTB

To investigate the neurodevelopmental role of CSTB (Fig. 1A; Supplementary Fig. S1), we generated a cell culture model of neural stem cell renewal and differentiation derived from the wild type (*wt*) and the *Cstb*$^{-/-}$ mouse brain (Fig. 1B). As previous data had implicated altered GABAergic signaling in *Cstb*$^{-/-}$ mice (Buzzi et al., 2012; Joensuu et al., 2014), we chose to model NPCs from the embryonic brain as their neurogenic potential in culture is largely restricted to GABAergic neurons (Sun et al., 2008). We carried out selective NPC amplification using low-passage neurosphere cultures (undifferentiated, uD) followed by a differentiation protocol for deriving neurons and glia within 12 days in culture (Fig. 1B).

Self-renewing and differentiating NPCs from *wt* mice expressed *Cstb,* which significantly increased during the differentiation protocol (Fig. 1C). A clonal colony-forming assay revealed that *Cstb*$^{-/-}$ NPCs present a significantly reduced self-renewal capacity in comparison to *wt* cells (Fig. 1D). Upon induction of differentiation, NPCs of both genotypes gave rise to an equal proportion of neurons. At day 12 post-differentiation (pD), approximately 21% of cells were immunopositive for doublecortin (DCX), expressed in neuroblasts and early differentiating neurons (Francis et al., 1999), whereas approximately 3% of cells expressed the neuron-specific class III β-tubulin (TUJ1) (Fig. 1E). TUJ1-expressing neurons were immunopositive for the neurotransmitter GABA. In turn, GABA-containing neurons expressed the vesicular GABA transporter (VGAT) (Supplementary Fig. S2). Immunostaining against the oligodendrocyte antigen O4 (Sommer and Schachner, 1981), we detected late oligodendrocyte precursors in low and variable frequency in both of the genotypes (Supplementary Fig. S3). By day 12 pD, the majority of cells acquired an astrocyte identity with robust expression of glial fibrillary acidic protein (GFAP) (Supplementary Fig. S4). During astrogliogenesis, the intermediate filament protein nestin becomes progressively downregulated with the accumulation of GFAP (Sergent-Tanguy et al., 2006). In the absence of CSTB, committed astrocytes underwent transition from a nestin$^+$ GFAP$^-$ to nestin$^-$ GFAP$^+$ expression at a faster rate than *wt* cells (Fig. 1F).

2.2. CSTB regulates histone H3 tail proteolysis during neural stem cell renewal and differentiation

Histone H3 tail cleavage has been observed in several cell identity transitions, including embryonic stem cell differentiation (Duarte et al., 2014; Duncan et al., 2008; Khalkhali-Ellis et al., 2014; Kim et al., 2016; Melo et al., 2017). In undifferentiated cells, CSTB localizes mainly to the nucleus, interacting with cathepsin L, a key protease linked to chromatin remodeling *via* proteolytic removal of the N-terminal tail of histone H3 (Adams-Cioaba et al., 2011; Alakurtti et al., 2005; Duncan et al., 2008; Riccio et al., 2001). We asked whether the same histone regulation occurs in NPCs. Using western blotting and a series of antibodies against histone H3 (Fig. 2A), we detected specific proteolysis upon induction of differentiation (Fig. 2B; Supplementary Fig. S5). Together, the data are consistent with cleavage events proximal to the lysine at position 27 (Fig. 2C, lighter cleaved band) and between alanine 21 and threonine 22, commonly known as H3 cleavage site 1 (H3cs1) (Duncan et al., 2008) (Fig. 2C, heavier cleaved band). Next, we explored the role of CSTB in modulating histone cleavage during NPC self-renewal and differentiation. In contrast to the wild type, we detected the H3cs1 band not only upon induction of differentiation, but also in undifferentiated NPCs (Fig. 2B), suggesting that CSTB-deficient cells undergo ectopic H3 tail proteolysis during self-renewal. Notably, the lighter cleavage band was absent in undifferentiated *Cstb*$^{-/-}$ NPCs (Fig. 2B), implying that its regulation, contrary to that of H3cs1, is independent from CSTB.

In order to test whether histone H3 tail cleavage occurs *in vivo* and is not due to a phenomenon induced by culturing cells, we analyzed brain extracts from *wt* and *Cstb*$^{-/-}$ E13.5 mouse embryos. We detected five-fold higher H3cs1 in the *Cstb*$^{-/-}$ brain samples (Fig. 2D). Progressive passage of neurospheres attenuated the abundance of H3cs1 independently of genotype but remained significantly elevated with CSTB deficiency (Fig. 2D), reflecting dysregulated histone cleavage in the absence of CSTB taking place both *in vivo* and at successive stages of *in vitro* NPC amplification.

Next, we characterized the H3cs1 at a cellular level. Upon differentiation, we observed that only a small fraction of *wt* cells were immunopositive for H3cs1 (Fig. 3A). The data imply that in *wt* cells H3 tail cleavage occurs transiently upon cellular induction. In contrast, differentiation of *Cstb*$^{-/-}$ NPCs led to a significant increase in the number of H3cs1$^+$ cells that remained constant over time (Fig. 3A). To test the specificity of CSTB in regulating the H3 tail cleavage pattern, we performed a rescue experiment with ectopic CSTB expression. Quantification of the transfected cells revealed a robust inhibition of H3 cleavage with CSTB overexpression (Fig. 3B), supporting a direct role for CSTB in this mechanism. Taken together, these data establish an essential function for CSTB in regulating cleavage of histone H3 at position T22 during neural stem cell renewal and differentiation.

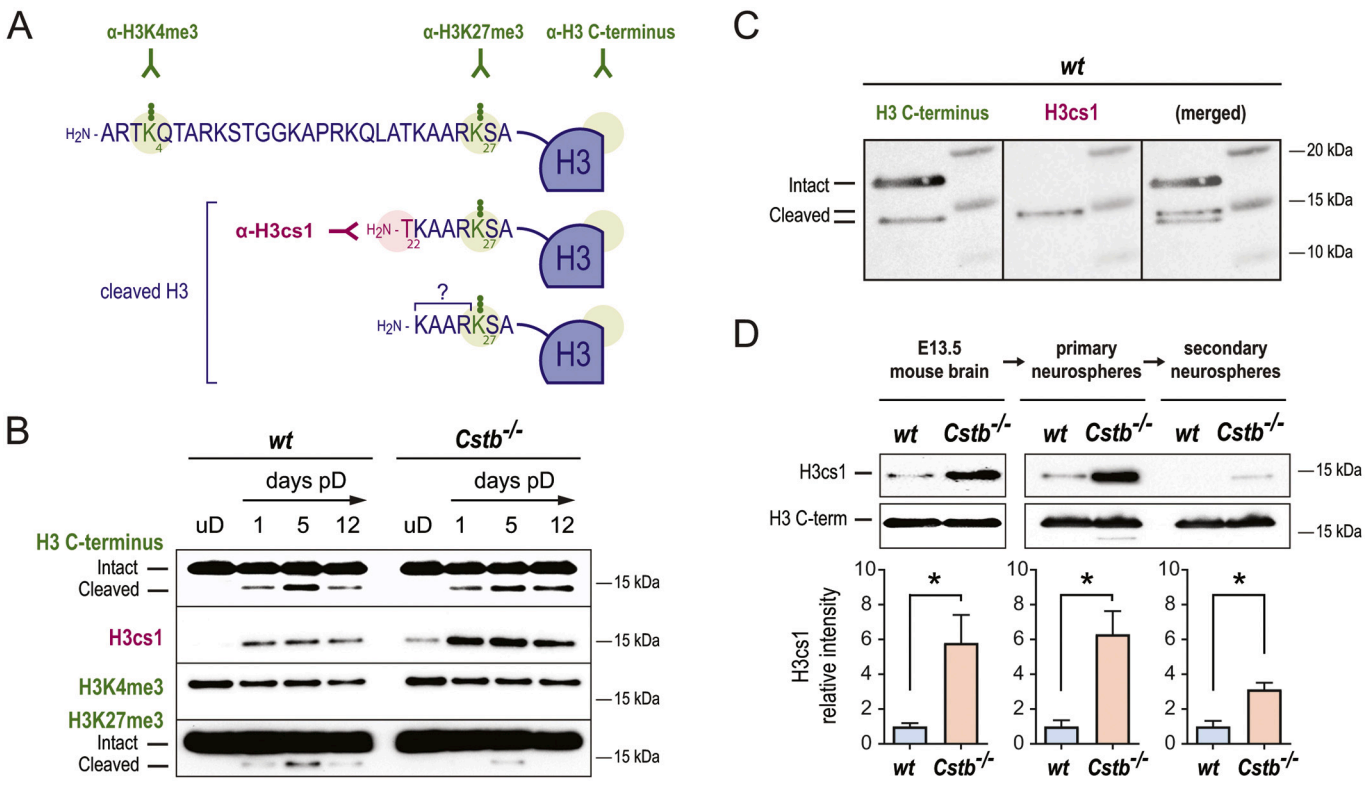

Fig. 2. CSTB-deficiency elicits premature histone H3 cleavage in self-renewing NPCs. A: N-terminal amino acid sequence of the different histone H3 products observed upon NPC differentiation and antibodies used to detect them. B: Western blot analysis of histone H3 in histone extracts collected from *wt* and *Cstb*$^{-/-}$ NPCs before induction of differentiation (uD) and at days 1, 5 and 12 after induction of differentiation (pD) using antibodies against the C-terminus of H3, H3cs1, H3K4me3 and H3K27me3. C: Sequential western blot detection of truncated products of histone H3 in *wt* NPCs at day 5 pD using antibodies against the C-terminus of H3 and H3cs1. D: Western blot analysis of the relative abundance of H3cs1 in histone extracts of *wt* and *Cstb*$^{-/-}$ E13.5 mouse embryo forebrains and cultured undifferentiated (uD) primary and secondary neurospheres. H3cs1 intensity value was normalized to that of total H3 and plotted as average ± SEM (E13.5 mouse brain: $n = 5$, $t_{(8)} = 2.968$, $p = 0.017$, t-test; primary neurospheres: $n = 3$–5, $t_{(4)} = 3.865$, $p = 0.018$, t-test; secondary neurospheres: $n = 3$–5, $t_{(6)} = 3.510$, $p = 0.013$, t-test).

2.3. Cathepsins B and L mediate ectopic histone H3 tail cleavage in CSTB-deficient neural precursor cells

CSTB is an endogenous inhibitor of cathepsin L, a previously established H3 tail protease in mouse embryonic stem cells (Duncan et al., 2008). To determine whether cathepsin L is responsible for H3 tail cleavage also in the neural cell lineage, we cultured undifferentiated *Cstb*$^{-/-}$ NPCs in the presence of the general cysteine protease inhibitor E-64 and the cathepsin B and L inhibitor *Z*-FF-FMK. In *Cstb*$^{-/-}$ cells cultured with either compound, H3cs1 was completely abolished (Fig. 4A), suggesting that CSTB inhibition of cathepsin L and/or cathepsin B regulates H3 tail cleavage. To differentiate between these two cathepsin proteases, we cultured *Cstb*$^{-/-}$ NPCs in the presence of the selective cathepsin B inhibitor CA-074 (Montaser et al., 2002). Interestingly, treatment with this compound caused a partial but significant decrease in the abundance of H3cs1 (Fig. 4A). Next, we measured the enzymatic activity of cathepsins L and B in whole cell lysates of *wt* and *Cstb*$^{-/-}$ NPCs using protease-specific fluorescent substrates. In *Cstb*$^{-/-}$ cells, we detected an increase in the activity of both cathepsins (Fig. 4B). Furthermore, addition of the cathepsin B inhibitor CA-074 strongly suppressed cathepsin B activity in NPCs (Fig. 4C). Taken together, the data strongly suggest that CSTB regulates cathepsins B and L histone H3 tail cleavage in NPCs.

2.4. Histone H3 tail cleavage is most frequent in cells committed to a neuron fate

As CSTB and the nuclear isoform of cathepsin L were previously shown to modulate the length of the cell cycle in a synchronized cancer cell line (Ceru et al., 2010), we tested whether histone cleavage is associated with cell proliferation. Differentiating NPCs were stained for Ki-67, a marker for actively proliferating cells (Gerdes et al., 1983). The proportion of cells immunopositive for both H3cs1 and Ki-67 was low both in *wt* and *Cstb*$^{-/-}$ NPCs (Fig. 5A) implying that H3 cleavage is most prevalent in non-dividing cells.

To elucidate whether histone cleavage is restricted to specific cell types, we stained differentiating NPCs for a number of cellular identity markers and quantified their co-localization with the antibody against H3cs1. A small percentage of H3cs1^{+} cells were immunopositive for nestin, a marker for dividing cells in early neuro- and gliogenesis or the astrocyte marker GFAP. In contrast, the majority of H3cs1^{+} cells (on average 76%–94%) were negative for both markers (Supplementary Fig. S6). These data imply that H3cs1 is mostly confined to neurogenesis. We observed that cells undergoing histone cleavage, were enriched with the neuronal maker TUJ1 (Supplementary Fig. S7). Further analysis with an antibody against DCX revealed that the majority of *wt* H3cs1^{+} cells were immature committed neurons (Fig. 5B). In CSTB deficiency, histone cleavage was found to be less specific to DCX^{+} neurons than in *wt* (Fig. 5B). Together, the data show that histone cleavage was mostly confined to committed neurons and suggest a potential role for CSTB to regulate histone cleavage in a cell-type-specific manner.

Finally, we evaluated the presence of H3cs1 in cells of the oligodendrocyte lineage using an antibody against the premyelinating oligodendrocyte marker O4. To account for the low and variable generation of oligodendrocytes in our culture system (Supplementary Fig. S3), we normalized the absolute number of H3cs1^{+} O4^{+} cells to the

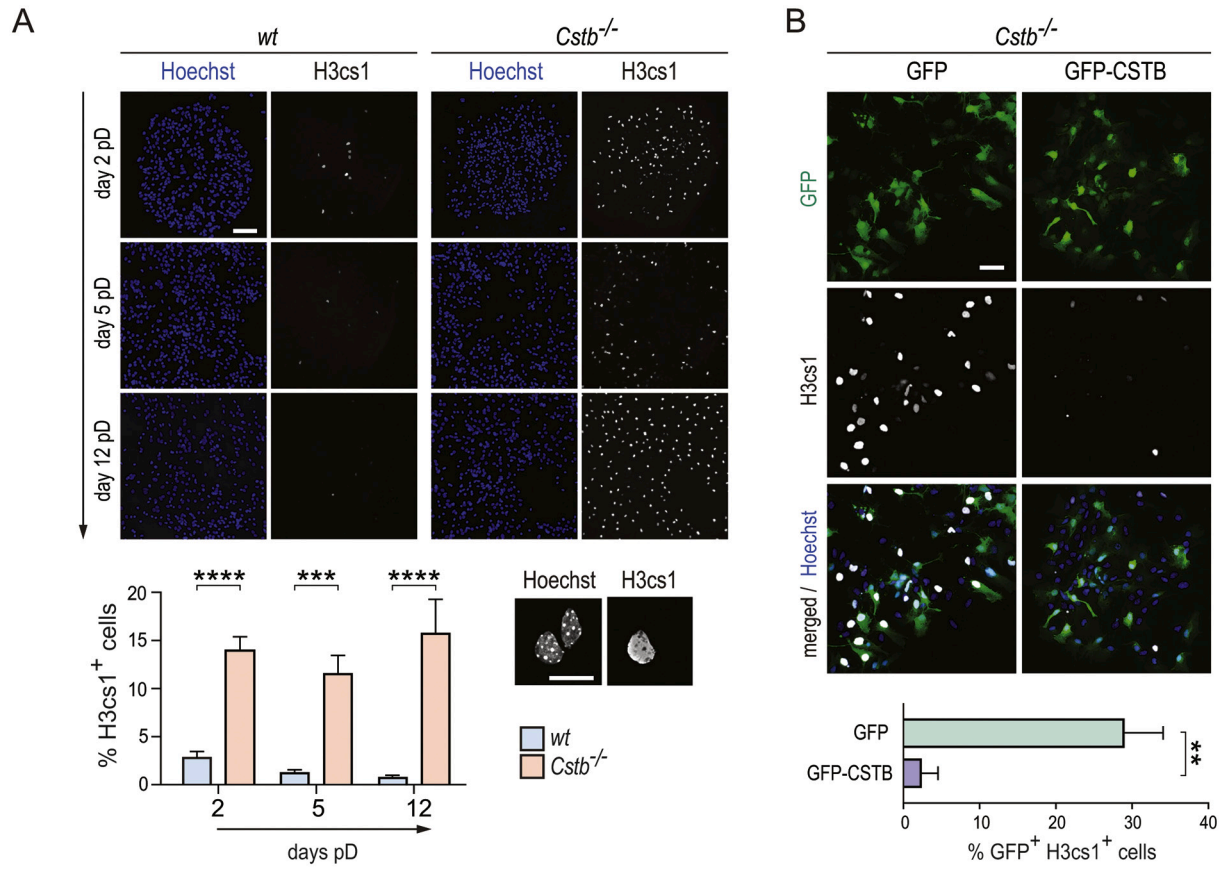

Fig. 3. CSTB modulates the proteolytic processing of histone H3 during neural stem cell differentiation. A: Representative immunofluorescence images of differentiating *wt* and $Cstb^{-/-}$ NPCs stained for H3cs1 and DNA (Hoechst). Scale bar = 100 μm. A confocal microscopy image depicting a H3cs1-positive cell and a H3cs1-negative cell is shown below. Scale bar = 20 μm. The chart depicts the average proportion of brightly-stained H3cs1-positive cells over total cell count ± SEM (n = 13–15; $F_{(5,78)} = 15.31$; $p < 0.0001$ at day 2 pD, $p = 0.0003$ at day 5 pD, $p < 0.0001$ at day 12 pD; One-way ANOVA). B: Representative immunofluorescence images of differentiating $Cstb^{-/-}$ NPCs overexpressing GFP or GFP-CSTB. Cells were stained for H3cs1 and DNA (Hoechst). Scale bar = 20 μm. The chart depicts the average proportion of H3cs1/GFP positive cells (both brightly- and faintly-stained) over the GFP positive cell count ± SEM ($n = 3$, $t_{(4)} = 4.683$, $p = 0.009$, t-test).

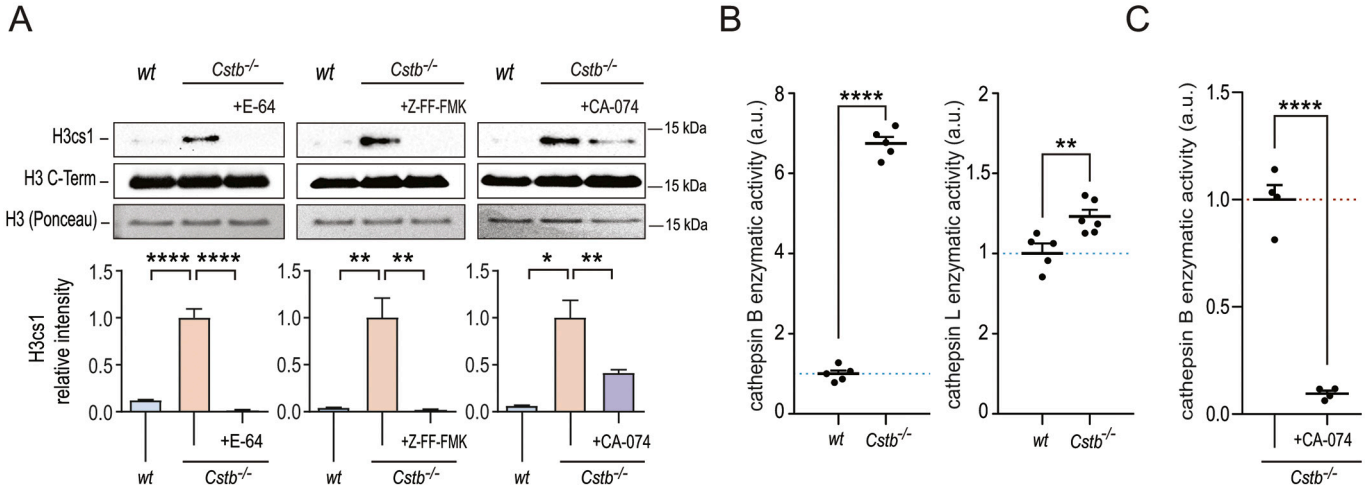

Fig. 4. Cathepsins B and L are responsible for ectopic histone H3 clipping in $Cstb^{-/-}$ NPCs. A: Western blot analysis and quantification of H3cs1 abundance in undifferentiated $Cstb^{-/-}$ NPCs treated with E64 (n = 4–8, $F_{(2,15)} = 174.6$, $p < 0.0001$, One-way ANOVA), *Z*-FF-FMK ($n = 3$, $F_{(2,6)} = 21.3$, $p = 0.003$, One-way ANOVA) and CA-074 ($n = 3$, $F_{(2,6)} = 18.66$, $p = 0.018$, One-way ANOVA). The capacity of each compound to block H3 tail cleavage was evaluated through comparison with corresponding vehicle-treated *wt* and $Cstb^{-/-}$ NPCs. H3cs1 intensity value was normalized to that of total H3, detected with an antibody against H3 C-terminus, and plotted as average ± SEM. Total H3 detected with Ponceau staining is also shown. B: Scatter plots depicting average enzymatic activity of cathepsins B and L in whole cell lysates of undifferentiated $Cstb^{-/-}$ NPCs in relation to *wt* levels (dotted lines) (n = 5–6; cathepsin B: $t_{(8)} = 31.95$, $p < 0.0001$; cathepsin L: $t_{(9)} = 3.48$, $p = 0.007$; t-test). C: Scatter plot depicting average enzymatic activity of cathepsin B in whole cell lysates of undifferentiated $Cstb^{-/-}$ NPCs treated with CA-074 in relation to vehicle-treated $Cstb^{-/-}$ control NPCs (dotted line) ($n = 4$, $t_{(6)} = 13.02$, $p < 0.0001$, t-test).

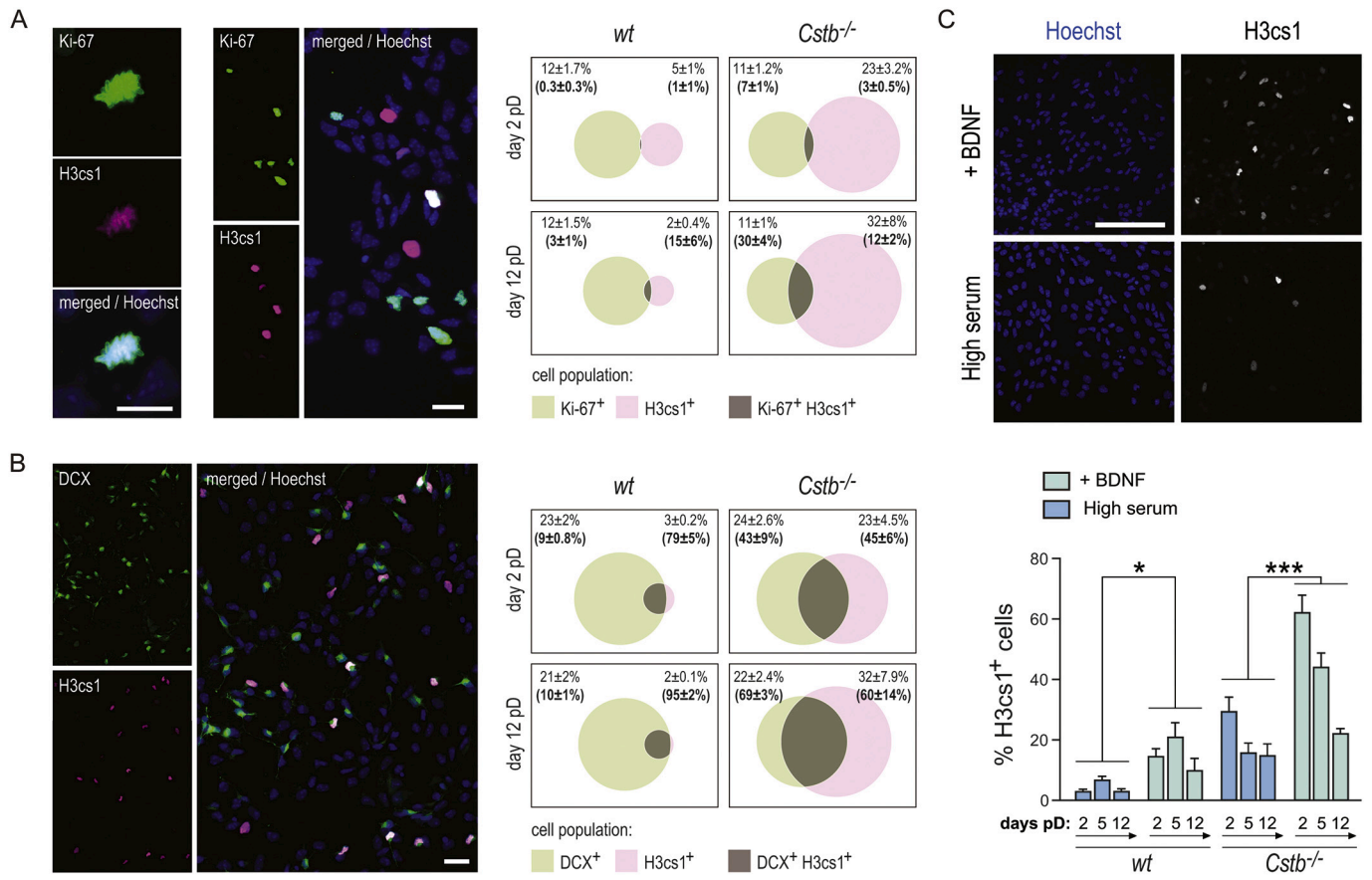

Fig. 5. Differentiation-associated H3 tail cleavage is most prevalent in committed neurons. A: Immunofluorescence images of differentiating *wt* NPCs at day 12 pD stained for Ki-67, H3cs1 and DNA (Hoechst). Colocalization shown in white. The left panel shows a Ki-67/H3cs1 positive cell at the prophase of mitosis. Scale bars = 20 μm. Venn diagrams depict overlap between Ki-67-positive and H3cs1-positive cell populations at the indicated time points in *wt* and in *Cstb*$^{-/-}$ cells. The upper percentages indicate the average size of the cell population relative to the total cell count ± SEM. The percentages in the parentheses indicate the proportion of H3cs1-positive cells immunopositive for Ki-67 as average ± SEM (n = 6). B: Representative immunofluorescence image of differentiating *wt* NPCs stained for doublecortin (DCX), H3cs1 and DNA (Hoechst). Colocalization shown in white. Scale bar = 20 μm. Venn diagrams depict overlap between DCX-positive and H3cs1-positive cell populations at the indicated time points, both in *wt* and in *Cstb*$^{-/-}$ cells. The upper percentages indicate the average size of the cell population relative to the total cell count ± SEM. The percentages in the parentheses indicate the proportion of H3cs1-positive cells immunopositive for DCX as average ± SEM (n = 5; DCX H3cs1 positive cells/H3cs1-positive cells between genotypes: $F_{(3,16)} = 7.308$; $p < 0.016$ at day 2 pD, $p = 0.015$ at day 12 pD; One-way ANOVA). C: Immunofluorescence images of differentiating *wt* NPCs at day 5 pD cultured in media supplemented with BDNF (+ BDNF) or containing a high concentration of serum (High serum) stained for H3cs1 and DNA (Hoechst). Scale bar = 50 μm. A chart depicts the percentage of H3cs1-positive cells over total cell count at the indicated time points in *wt* (n = 4; $F_{(1,6)} = 13.57$; $p < 0.0103$; Two-way ANOVA) and in *Cstb*$^{-/-}$ cells (n = 4; $F_{(1,6)} = 75.23$; $p = 0.0001$; Two-way ANOVA) as averages ± SEM.

total O4$^+$ cell count. We found that 2%–7% of O4$^+$ *wt* cells were immunopositive for H3cs1, the proportion of H3cs1$^+$ O4$^+$ cells being significantly higher in CSTB-deficient conditions (40%–49%; Supplementary Fig. S8).

Collectively, our data show that all three major cell types of neural origin undergo H3 tail cleavage during differentiation with the mechanism most prevalent among cells committed to a neuronal fate. To gain further support to this interpretation, we induced NPC differentiation in media containing brain-derived neurotrophic factor (BDNF) to promote neuronal differentiation or high serum concentrations to depress it. The experimental setup was validated through quantification of TUJ1$^+$ and GFAP$^+$ cells at day 12 pD (Supplementary Fig. S9). Staining for H3cs1 revealed that both *wt* and *Cstb*$^{-/-}$ NPCs cultured in BDNF-supplemented media displayed a significantly higher number of H3cs1$^+$ cells, consistent with enhanced production of neurons (Fig. 5C).

2.5. Time-resolved transcriptional changes in *Cstb*$^{-/-}$ neural progenitor cells

Promoter-associated H3 tail cleavage facilitates induction of gene expression in yeast (Santos-Rosa et al., 2009). To address whether histone cleavage in NPC was accompanied by transcriptional changes, we used RNA sequencing (RNAseq) from mRNAs isolated of NPC populations during self-renewal and following the induction of differentiation. A principal component analysis (PCA) of the transcriptomics data showed that approximately 93% of the variation between samples originated from the process of differentiation rather than the genotype (Fig. 6A; Supplementary Fig. S10). The samples derived from undifferentiated NPCs formed a tight cluster, reflecting a high degree of similarity between their transcriptomes. However, PCA of this timepoint alone consistently separated *wt* and *Cstb*$^{-/-}$ samples along the PC1 axis (32% of the variation) (Fig. 6A), indicating that the transcriptional alterations associated with CSTB deficiency manifest before the induction of differentiation, coinciding with premature histone cleavage.

Comparative transcriptome analysis of undifferentiated NPCs revealed a total of 112 differentially expressed genes (DEGs) (Fig. 6B and Supplementary Table S1), of which 97 were upregulated in *Cstb*$^{-/-}$ NPCs. A bioinformatic analysis of these 112 genes using Gene Ontology (GO) enrichment analyses revealed enrichment of processes related to cytoplasmic and mitochondrial protein synthesis and control of protein translation. We also noted an enrichment in RNA metabolism-related genes linked to processing and splicing of pre-mRNAs. Furthermore,

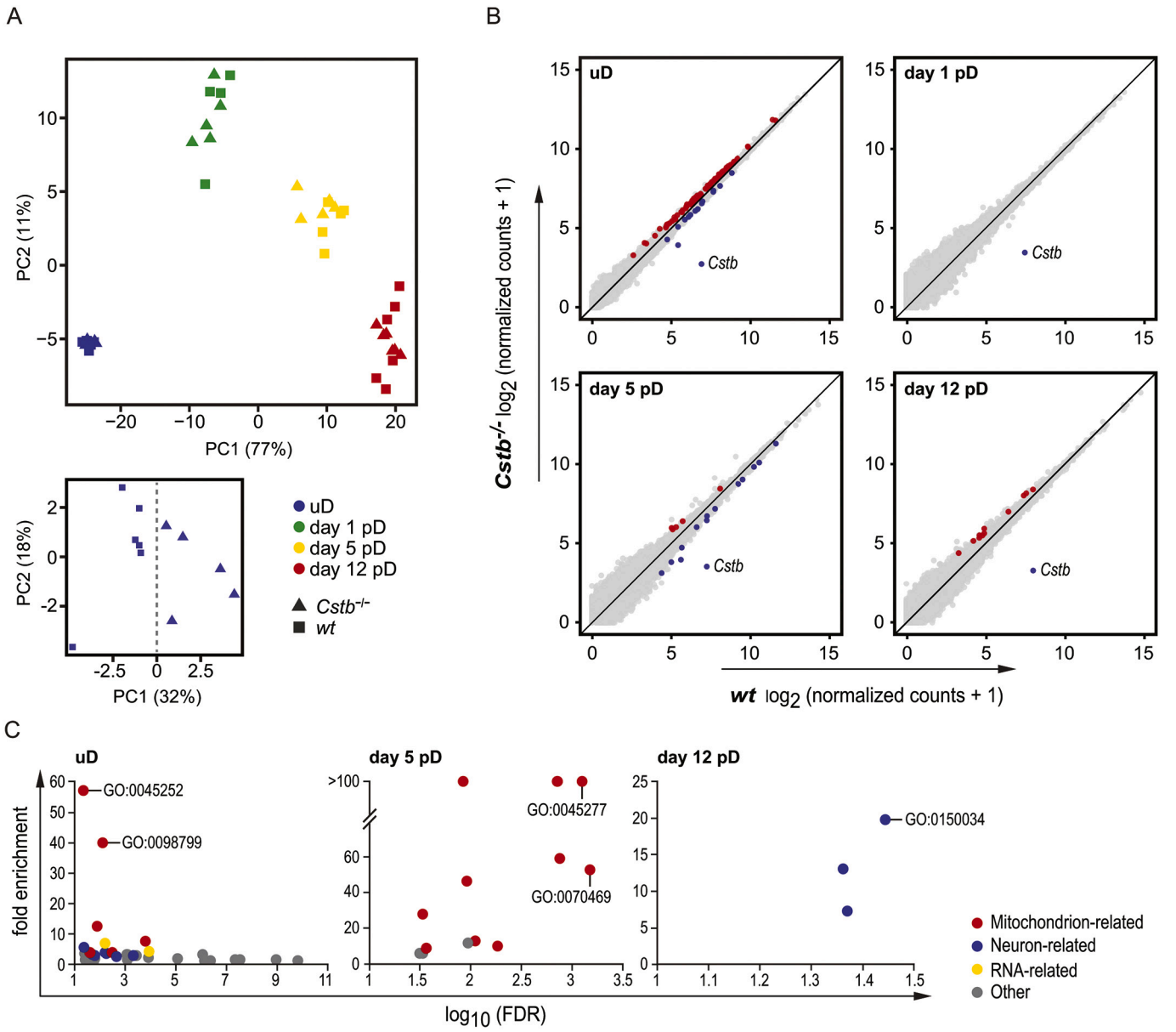

Fig. 6. Transcriptional changes during self-renewal and differentiation in *Cstb*$^{-/-}$ NPCs. A: PCA of all 42 mRNA samples analyzed by RNAseq. PCA of undifferentiated samples alone is also displayed. B: Scatter plots depicting all expressed genes per timepoints analyzed. X-axis and Y-axis represent mean gene expression in *Cstb*$^{-/-}$ and *wt* mRNAs, respectively. Red and blue dots depict the significantly upregulated and significantly downregulated genes in *Cstb*$^{-/-}$ samples, respectively. C: Dot charts depicting GO Cellular Component annotations with a statistically significant enrichment among differentially expressed gene datasets in *Cstb*$^{-/-}$ at the indicated timepoints. Each category is represented as a dot plotted in relation to its significance level (base 10 logarithm of the false discovery rate ($\log_{10}$FDR), X-axis) and its fold-enrichment in the dataset (Y-axis). Colored dots represent categories related to mitochondrion, neuron and RNA metabolism as indicated. Examples of top-ranking categories: oxoglutarate dehydrogenase complex (GO:0045252), outer mitochondrial membrane protein complex (GO:0098799), respiratory chain complex IV (GO:0045277), respirasome (GO:0070469), distal axon (GO:0150034). (For interpretation of the references to colour in this figure legend, the reader is referred to the web version of this article.)

GO cellular components identified 30 mitochondrion-associated genes (Fig. 6C and Supplementary Table S2).

2.6. *Defective mitochondrial respiration in differentiating Cstb*$^{-/-}$ *NPCs*

To characterize the enrichment of functionally related gene sets in the NPC transcriptomes, we ranked all DEGs by expression fold change and carried out gene set enrichment analysis (GSEA). We found that, specifically at days 1 and 5 following induction of differentiation, genes belonging to the GO term "electron transport chain" were significantly enriched at the left pole of the ranking, indicating reduced expression in *Cstb*$^{-/-}$ NPCs (Fig. 7A). We confirmed the reduced expression of electron transport chain genes by RT-qPCR (Supplementary Fig. S11). To address the functional consequence of this gene expression regulation, we turned to high-resolution respirometry of NPCs to assess oxidative phosphorylation. In undifferentiated cells, mitochondrial respiratory function was not altered between genotypes (Fig. 7B). The induction of differentiation stimulates a significant increase in the oxygen consumption rate of the cells, which is delayed with CSTB-deficiency (Fig. 7B). This suggests the onset of mitochondrial dysfunction in *Cstb*$^{-/-}$ cells.

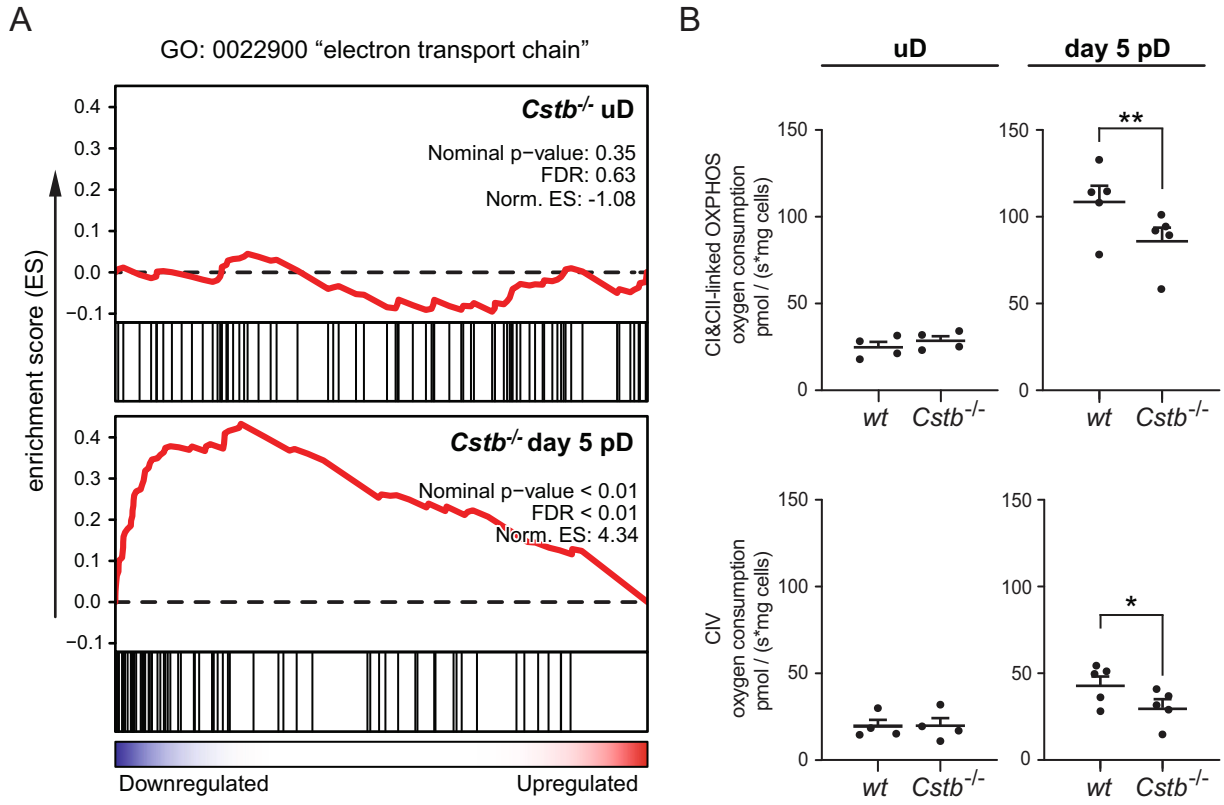

Fig. 7. Mitochondrial dysfunction upon differentiation of *Cstb*$^{-/-}$ NPCs. A: GSEA of differentially expressed genes in *Cstb*$^{-/-}$ NPCs for the GO term "electron transport chain" before differentiation (uD) and during differentiation (day 5 pD). Genes are ranked from left to right from the most downregulated to the most upregulated in *Cstb*$^{-/-}$ NPCs, respectively (one black line = one gene). B: Mitochondrial respiratory capacity measurements using high-resolution respirometry in *wt* and *Cstb*$^{-/-}$ NPCs before and during differentiation. The scatter plots depict the average rate (± SEM) of oxygen consumption (pmol/s) by maximally coupled respiration (state III) through oxidative phosphorylation complexes I and II (CI&CII-linked OXPHOS) and individually assessed IV (CIV) normalized to protein input ($n = 5$; C1&CII-linked OXPHOS: $t_{(4)} = 5.303$, $p = 0.006$, paired t-test; CIC: $t_{(4)} = 4.276$, $p = 0.013$, paired t-test).

3. Discussion

In the present study, we establish the cysteine protease inhibitor CSTB as a regulator of chromatin structure. We show that CSTB modulates the proteolytic cleavage of the N-terminal tail of histone H3 during neural stem cell differentiation. Absence of CSTB leads to premature initiation of H3 tail cleavage in undifferentiated neural progenitors and impaired mitochondrial respiratory function in differentiating cells. Our findings have important implications to the molecular pathogenesis of CSTB dysfunction, revealing the origins of epigenetic regulation in the associated human diseases.

CSTB was found to specifically regulate H3 tail cleavage at threonine 22 by cathepsins B and L. Proteolytic processing of histone H3 at this site is an evolutionary conserved mechanism previously linked to a multitude of cellular functions, namely yeast sporulation and starvation, malaria parasite infection, mammalian embryonic stem cell differentiation, and oncogene-induced senescence (Duarte et al., 2014; Duncan et al., 2008; Herrera-Solorio et al., 2019; Santos-Rosa et al., 2009; Vossaert et al., 2014). Our data demonstrate that this mechanism is also pivotal in timing the induction of differentiation of neural progenitor cells with CSTB delimiting the temporal window and cell-type specificity of the proteolytic event. Despite H3cs1 being the best described modality of histone H3 tail cleavage, little is known about the upstream molecular mechanisms. Our study provides an important contribution to the understanding of these mechanisms, revealing CSTB as an endogenous regulator of histone cleavage and linking this process to human brain diseases. Over a dozen enzymes have been shown to proteolytically process the N-terminal tail of histone H3 in a biological context (Yi and Kim, 2018). Of these, only cathepsin L and an as yet unidentified serine protease involved in yeast sporulation have been linked to H3cs1 (Duarte et al., 2014; Duncan et al., 2008; Santos-Rosa et al., 2009). Interestingly, our data strongly suggest that in NPCs cathepsin L and cathepsin B are responsible for H3cs1. This finding, therefore, identifies a third protease to this specific cleavage mechanism.

Considering the degree of complexity found in the mammalian brain, it is perhaps not unexpected to find redundancy in the machinery driving neural stem cell differentiation. Indeed, overlapping functions for these cathepsin proteases in the nervous system have previously been implicated in genetically modified mice lacking either cathepsin L or B. Single knockouts of either gene are viable, whereas double-knockouts develop severe brain atrophy and die shortly after birth (Felbor et al., 2002; Halangk et al., 2000; Nakagawa et al., 1998). Cathepsin B was recently shown to participate in chromosome segregation during mitosis (Hamalisto et al., 2020) through a mechanism of proteolytic processing of histone H3 in the C-proximal or globular domain. This requires direct leakage of lysosomes onto the chromatin upon disintegration of the nuclear envelope during mitosis. In contrast, the mechanism we establish here for H3 tail cleavage is intrinsically distinct and occurs preferentially in non-dividing cells. Together, the data support the view that a common group of enzymes has evolved to mediate both homeostatic and epigenetic signaling functions through histone degradation and tail cleavage, respectively, depending on the biological context (Dhaenens et al., 2015).

Our data imply that CSTB plays a dual role in the regulation of H3 tail cleavage. Proteolysis in *wt* NPCs was limited to the early stages of differentiation, whereas in *Cstb*$^{-/-}$ cells this occurred before the induction of differentiation and persisted throughout differentiation. Neural cells lacking CSTB are thus exposed to the continuous removal of histone tails

following terminal differentiation. Considering that histone cleavage is largely restricted to cellular identity transitions (Duncan et al., 2008; Khalkhali-Ellis et al., 2014; Kim et al., 2016), sustained removal of histone tails will likely interfere with the establishment of histone post-translational modification profiles characteristic of differentiated neural cells. Interestingly, H3cs1 has been shown to drive a cellular senescence program in human fibroblasts and melanocytes (Duarte et al., 2014). Notably, cleaved H3 species were nucleosomal in senescent cells and ectopic expression on the cleaved histone was sufficient to trigger its downstream chromatin effects following incorporation into the chromatin mediated by an endogenous histone chaperone machinery. These findings are in line with a more recent study in the human malaria parasite indicating that the proteolytic processing of histone H3 can precede its incorporation into specific genomic loci involved in DNA replication (Herrera-Solorio et al., 2019). This implies that chromatin integration of the cleaved H3 products occurs independently of whether the cleavage takes place in the nucleosomal or in the free pool of histone H3. Thus, the genomic distribution of truncated H3 products in neural cells and the functional consequences of H3cs1 need to be explored in future studies.

We report a slight but significant decrease in the self-renewing capacity of CSTB-deficient NPCs, coinciding with premature initiation of histone H3 cleavage before induction of differentiation. Upon differentiation, H3cs1 was mostly confined to immature neurons. Nonetheless, we did not detect any alteration in the neurogenic potential of cells lacking CSTB. A recent study reported premature differentiation in EPM1 patient derived brain organoids, evidenced by decreased progenitor proliferation, increased numbers of immature neurons and smaller organoid sizes. Additionally, CSTB-deficiency was reported to impair neuronal migration in the embryonic mouse brain (Di Matteo et al., 2020). Neuronal migration is preceded by dysregulated histone cleavage in the E13.5 *Cstb*$^{-/-}$ mouse brain, suggesting a causal relationship between both phenotypes. Combined, the data support the notion that CSTB has a more crucial role in human than in mouse brain development. This is in line with the observation that *CSTB* null mutations cause a rapidly progressing microcephaly in humans, manifesting soon after birth (Mancini et al., 2016; O'Brien et al., 2017), whereas the progression of brain atrophy in *Cstb*$^{-/-}$ mice is more protracted (Joensuu et al., 2014; Manninen et al., 2014; Pennacchio et al., 1998; Shannon et al., 2002; Tegelberg et al., 2012), with deterioration of motor functions appearing later during disease course. These data are in accordance with previous reports on single gene defects linked to microcephaly in humans presenting a milder phenotype in mice (Chen et al., 2014; Pulvers et al., 2010; Trimborn et al., 2010) and suggest that the human brain is especially vulnerable to genetic mutations interfering with NPC renewal and differentiation.

Cleavage of histone H3 between amino acids 21 and 22 has previously been linked to the regulation of gene expression (Duarte et al., 2014; Santos-Rosa et al., 2009). Transcriptome profiling of undifferentiated *Cstb*$^{-/-}$ NPCs identified subtle but significant transcriptional changes in over a hundred genes. The majority of these genes were upregulated, in agreement with previously studies linking H3 tail cleavage with transcriptional activation (Kim et al., 2016; Santos-Rosa et al., 2009). We detected a robust enrichment in nuclear encoded mitochondrial genes, representing approximately a quarter of the upregulated genes in undifferentiated *Cstb*$^{-/-}$ cells. The process of neurogenesis involves a robust upregulation of mitochondrial biogenesis, which is part of the metabolic transition from aerobic glycolysis to mitochondrial oxidative phosphorylation (Agostini et al., 2016; Zheng et al., 2016). Consistently, we detected an increase in the mitochondrial respiratory capacity of differentiating *wt* NPCs. In contrast, *Cstb*$^{-/-}$ cells exhibited a delayed upregulation of mitochondrial respiration, accompanied by a generalized downregulation of electron-transport-chain genes. The divergent transcriptional signatures of *Cstb*$^{-/-}$ NPCs during self-renewal and differentiation could indicate that H3cs1 plays a more intricate role in transcriptional regulation than merely facilitating gene expression. Further studies targeting the genomic distribution of H3cs1, both in physiological conditions and in the absence of CSTB, are needed to clarify the relationship between CSTB, histone cleavage and transcriptional regulation, particularly that of nuclear-encoded mitochondrial genes. Mitochondrial metabolism is a cornerstone of neuronal homeostasis and has profound implications for both neuronal development and disease (Iwata et al., 2020; Styr et al., 2019). The central role for epigenetic mechanisms in the regulation of mitochondrial biogenesis upon NPC differentiation has only recently began to be uncovered (Uittenbogaard et al., 2018). Considering that H3cs1 is mostly confined to immature neurons, it is tempting to speculate that histone cleavage participates in the epigenetic regulation of their metabolic program. Recently, proteomics analysis of synaptosomes isolated from preclinical *Cstb*$^{-/-}$ mouse cerebella revealed altered abundance of mitochondrial proteins as a key finding (Gorski et al., 2020). These data are in line with our RNA sequencing findings, and collectively suggest that early mitochondrial dysfunction might be a critical factor in the pathogenesis of CSTB deficiency. Notably, the overlap between the proteomics data of synaptosomes and the RNA sequencing data in NPCs also extends to other functional categories, highlighting alterations in intracellular transport and protein translation. The data of the present study strongly suggest that these changes originate at the early stages of neuronal fate specification, probably due to defective regulation of gene expression at neural progenitor stages.

Our findings constitute the earliest molecular changes reported in *Cstb*$^{-/-}$ mice, implying a key role for epigenetic alterations in triggering the pathogenesis associated with CSTB deficiency. They provide a likely explanation for the striking genotype-phenotype correlations linked to biallelic loss of CSTB function in humans (Lalioti et al., 1997; Mancini et al., 2016). Of interest, EPM1 patients with a partial loss of function have apparently normal brain development while the key pathology of progressive neurodegeneration typically presents in late childhood-early adolescence (Pennacchio et al., 1996). How a moderate level of H3cs1 contributes to EPM1 pathogenesis needs to be explored in future studies. The link between histone H3 cleavage and neurologic disease established here through CSTB adds a new mechanistic view to the growing number of “chromatinopathies”, neurodevelopmental diseases caused by disrupted chromatin structure (Ciptasari and van Bokhoven, 2020; Lewis and Kroll, 2018).

In conclusion, our data support a model whereby CSTB-deficiency affects the structure of histone H3 during brain development subsequently laying the foundation for impaired cellular homeostasis. Collectively, our findings provide novel insights into the early onset and pathogenesis of CSTB-deficiency and reveal greater complexity to the molecular pathogenesis of EPM1.

4. Materials and methods

4.1. Mouse model

The *Cstb*$^{-/-}$ mouse strain used in this study is 129S2/SvHsd5-*Cstb*^{tm1Rm}, derived from the Jackson Laboratory strain 129-*Cstb*^{tm1Rm}/J (stock no. 003486; https://www.jax.org/strain/003486) (Pennacchio et al., 1998). Wild type (*wt*) mice of the same age and background were used as controls. The research protocols were approved by the Animal Ethics Committee of the State Provincial Office of Southern Finland (decisions ESAVI/10765/04.10.07/2015 and ESAVI/471/2019).

4.2. Primary cell cultures

The ganglionic eminences of E13.5 mouse embryos were mechanically dissociated and plated at 2×10^5 cells/ml in 5 ml maintenance media: Dulbecco's modified Eagle's media (DMEM):F12 (3:1), 2% B-27, 20 ng/ml EGF (Millipore), 40 ng/ml mouse FGF-basic (PeproTech) (Ciccolini and Svendsen, 1998). For passaging, neurospheres were dissociated with TrypLE Express (Gibco) and cultured in maintenance

media at 6 × 10^4 cells/ml. Experiments were carried out with passage two neurospheres, unless otherwise specified. To determine the capacity of individual NPCs to form a secondary neurosphere (clonal colony-forming assay), single cell suspensions derived from primary neurospheres were plated onto 96-well plates at a density of 3, 5, 7 or 9 cells/well and cultured for 8 days prior to colony enumeration using a phase-contrast microscope. Cell viability discrimination and plating was carried out using flow cytometry. For differentiation, cells were plated onto poly-ornithine-coated surfaces at 3 × 10^4 cells/cm^2 in differentiation media; Standard: Neurobasal media (NB), 2% B-27, 2% fetal bovine serum (FBS); BDNF-supplemented media: NB, 2% B-27, 0.5% FBS, 30 mM glucose, 100 ng/ml BDNF (PeproTech) and 50 ng/ml bovine serum albumin (BSA) (Silva et al., 2009; Torrado et al., 2014); High-serum media: NB, 2% B-27, 10% FBS (Brunet et al., 2004). For protease inhibitor assays neurospheres were grown with 5 μM E-64 (in H_2O), 10 μM *Z*-FF-FMK (in DMSO), 10 μM CA-074 (in DMSO) (Merck) or corresponding vehicle for four days prior to harvesting.

4.3. Histone extraction and western blotting

Bulk histones were isolated from cells or tissue using Histone Extraction Kit (Abcam) and resolved on 4–12% Bis-Tris Plus Bolt™ gels at 4–5 μg of protein per lane in MES SDS Running Buffer (Invitrogen). Target-protein signal was detected with Horseradish Peroxidase (HRP) -conjugated secondary antibodies, followed by chemiluminescence reaction and image acquisition using ChemiDoc MP and Image Lab (v6.0; Bio-Rad). For normalization, membranes were gently stripped, re-blocked and re-probed against histone H3 C-terminus.

4.4. Enzymatic activity assays

Substrate-based fluorometric enzymatic activity assays were performed on fresh whole cell lysates of undifferentiated NPCs using Cathepsin L Activity Assay Kit (Abcam) and Cathepsin B Activity Assay Kit (Abcam).

4.5. Immunocytochemistry

Neurospheres were plated onto 12 mm German glass coverslips (Bellco) and cultured in differentiation media for up to 12 days. Cells were fixed with 4% PFA for 15 min at RT, followed by permeabilization with 0.1% Triton X-100 for 10 min. Hoechst 33342 (1:2000) was used to counterstain the nuclei.

4.6. Antibodies

Primary antibodies used: rabbit α-H3 C-terminus (Abcam, Western blot (WB) 1:15000, RRID: AB_302613), rabbit α-H3cs1 (Cell Signaling Technologies, WB 1:1000, immunocytochemistry (ICC) 1:500, RRID: AB_2797961), rabbit α-H3K4me3 (Abcam, WB 1:2000, RRID: AB_306649), rabbit α-H3K9me3 (Abcam, WB 1:3000, RRID: AB_2797591), rabbit α-H3K27me2 (Abcam, WB 1:4000, RRID: AB_448222), mouse α-Nestin (Millipore, ICC 1:100, RRID: AB_94911), rabbit α-GFAP (Agilent Technologies, ICC 1:200, RRID: AB_10013382), rat α-GFAP (Thermo Fisher Scientific, ICC 1:500, RRID: AB_2532994), mouse α-DCX (Santa Cruz Biotechnology, ICC 1:150, RRID: AB_10610966), mouse α-βIII-tubulin (TuJ1) (Millipore, ICC 1:500, RRID: AB_2210524), rabbit α-GABA (Sigma-Aldrich, ICC 1:10000, RRID: AB_477652), mouse α-VGAT (Synaptic Systems, ICC 1:1000, RRID: AB_887872), mouse α-O4 (Millipore, ICC 1:200, RRID: AB_11213138), rat α-Ki-67 (Thermo Fisher Scientific, ICC 1:200, RRID: AB_10853185). For WB, HRP-conjugated swine α-rabbit (Agilent Technologies, RRID: AB_2617141) was used at 1:8000 to detect α-H3 C-terminus and at 1:5000 for all other antibody targets. For ICC, fluorescently labeled secondary antibodies (Alexa Fluor 488, 594 and 647; Thermo Fisher Scientific) were used at 1:500.

4.7. Expression plasmids and transient transfections

To produce EGFP-CSTB fusion protein, the coding sequence of *CSTB* was cloned into an EGFP expression vector (pEGFP-N3, Clontech, GenBank: U57609). The empty EGFP vector was used as a control. C-terminal tagging of CSTB was chosen to prevent interaction with the protease recognition domain found near the N-terminus of the protein. Plasmid delivery through electroporation of passage three neurospheres was performed using Mouse neural stem cell nucleofector kit (Lonza).

4.8. RNA sequencing

4.8.1. Sample collection and library preparation

A total of 44 neurospheres from three independent cultures were harvested and lysed directly or plated for differentiation in round-bottom 96-well plates and lysed after 1, 5 or 12 days. To limit the variability arising from clonal heterogeneity (Suslov et al., 2002), we focused the study on middle-sized neurospheres (approx. 200 μm, 400 cells). Cell lysis in Tris buffer (pH 7) containing 1% SDS, 10 mM EDTA and 0.2 mg/ml Proteinase K was followed by RNA extraction with RNA Clean & Concentrator kit (Zymo). 48-plex RNAseq libraries were prepared using modified STRT method with unique molecular identifiers (UMIs) (Islam et al., 2011; Islam et al., 2014). In order to remove amplification artefacts at high copy numbers, we used longer UMIs of 8 bp. To increase the coverage, the libraries were sequenced twice with Illumina NextSeq 500, High Output (75 cycles).

4.8.2. STRT RNAseq data preprocessing

The raw output base call (BCL) files were demultiplexed with Picard (v2.10.10) ExtractIlluminaBarcodes and IlluminaBasecallsToSam to generate unaligned BAM files. BAM files were converted to FASTQ files with Picard SamToFastq and aligned to the mouse reference genome mm10, mouse ribosomal DNA unit (GenBank: BK000964), and ERCC spike-ins (SRM 2374) with the GENCODE (vM19) transcript annotation using HISAT2 (v2.1.0) (Kim et al., 2019). Aligned BAM files were merged with the original unaligned BAM files to generate UMI-annotated BAM files by Picard MergeBamAlignment. BAM files corresponding to each sample from different lanes and runs were merged using Picard MergeSamFiles. Potential PCR duplicates were marked with Picard Markduplicates. The resulting BAM files were processed with featureCounts (v1.6.2) (Liao et al., 2014) to assign the reads to 5′-end of genes. Uniquely mapped reads within the 5′-UTR or 500 bp upstream of protein-coding genes based on the NCBI RefSeq protein-coding genes and the first 50 bp of spike-in sequences were counted. FASTQ files after exclusion of duplicated reads have been deposited in the ArrayExpress database at EMBL-EBI under accession number E-MTAB-8934. The numbers of total and of mapped reads for each sample are summarized in Supplementary Table S3.

4.8.3. RNAseq expression data analysis

Two samples out of the total 44 samples were excluded due to the extremely low number of mapped reads. After filtering out lowly expressed genes and spike-ins, differential expression analysis between *wt* and $Cstb^{-/-}$ samples at each timepoint was performed with the 'nbinomWaldTest' method of an R (v3.5.2) package DESeq2 (v1.22.2) (Love et al., 2014), which uses the Benjamini-Hochberg procedure to adjust the *p*-values for multiple testing (Benjamini and Hochberg, 1995). Genes with adjusted *p*-value less than 0.05 were considered as significantly differentially expressed. Principal component analysis was performed using the 500 genes with the highest variance across all the 42 samples. Gene set enrichment analysis (GSEA) was performed with GSEA (v4.0.3) using GSEAPreranked tool (Subramanian et al., 2005), where genes were preranked based on their *p*-values and fold changes. Mouse gene sets for Gene Ontology were downloaded from http://ge-lab.org/gskb/. GSEA plots were generated using ReplotGSEA.R with some modifications. Gene ontology terms of GO biological

processes, GO cellular components and GO molecular functions significantly enriched in our datasets were calculated using Fisher's exact test with Benjamini-Hochberg correction using web-based tools WebGestalt (version 01/14/2019) (Liao et al., 2019), Ingenuity Systems Pathway Analysis (IPA, QIAGEN, version 01-14) and the GO Ontology Resource (version 2019-12-09).

4.9. Real-Time PCR

Total RNA was isolated with NucleoSpin RNA Plus kit (Macherey-Nagel) and reverse-transcribed with iScript cDNA synthesis kit (BioRad). RT-qPCR was performed in CFX96 Real-Time System (Bio-Rad) using TaqMan Fast Advanced Master Mix (Applied Biosystems). The following TaqMan probes were used for target amplification: *Cstb* (Mm00432769_m1), *Rpl19* (Mm02601633_g1), *Uqcrfs1* (Mm00481849_m1), *Ndufs2* (Mm00467603_g1). Gene expression data was normalized to that of genes *Atp5c1* (Mm00662408_m1) and *Ywhaz* (Mm03950126_s1), chosen based on RNA sequencing data for their high and stable expression among timepoints and genotypes. Relative gene expression was calculated using the $2^{-\Delta Ct}$ method. All primers were validated, and RT-qPCR assays were performed in accordance with MIQE guidelines.

4.10. High-resolution respirometry

Oxygen consumption rates were measured using a substrate-uncoupler-inhibitor protocol on a high-resolution oxygraph (Oroboros Instruments) as previously described (Jackson et al., 2014). Briefly, neurospheres were dissociated with TrypLE express, resuspended in respiration buffer (110 mM D-sucrose, 60 mM lactobionic acid, 20 mM HEPES, 20 mM taurine, 10 mM KH_2PO_4, 3 mM $MgCl_2$, 0.5 mM EGTA, 1 g/l fatty acid-free BSA, pH 7.1) and loaded at 2×10^6 cells per chamber. Measurements were carried out in duplicates. Cells were digitonin-permeabilized, and oxygen consumption rates assessed in the presence of pyruvate-glutamate-malate with specific activities determined with +ADP, and +succinate (CI&CII-linked maximal coupled respiration, state III), maximal uncoupled respiration by titration of FCCP and individual assessment of complex IV by +Asc/TMPD (CIV). Specific oxygen consumption rates are expressed as pmol/s per million cells. For respirometry of day 5 pD samples, cells were washed with PBS, collected by scraping directly in respiration buffer and analyzed as described above with input normalized to amount of protein.

4.11. Experimental design and statistical analysis

A biological replicate (n) was defined as a cell culture or tissue sample derived from an independent pool of mouse embryos (3 to 5 individuals from the same litter). In every case, at least three biological replicates were analyzed per condition (timepoint and genotype). Immunostained cell cultures were imaged with Zeiss Axio Imager M2 microscope equipped with Axiocam 503 camera (Zeiss). Sample sizes of five or more biological replicates were used. For every biological replicate and condition, 10 random fields were captured with 20× or 40× objective. Cell numbers were quantified manually in ZEN software (Zeiss, v2.3). Total number of cells per field was defined by number of nuclei, counted manually or with automated thresholding in ImageJ software.

Statistical analyses were carried out with GraphPad Prism (v5.0a) or with R Studio software. Comparisons between experimental conditions were made using Student's t-test (unpaired unless otherwise specified), one-way ANOVA with Bonferroni correction, two-way ANOVA with Greenhouse-Geisser correction or linear mixed model followed by Wald's chi square test depending on the experimental setup. Differences between groups were considered statistically significant when $p < 0.05$.

Declaration of Competing Interest

None.

Acknowledgements

We acknowledge Veronika Rezov for her skilled technical assistance, Katarin Gorski for technical advice and Brendan Battersby for critical reading of the manuscript. We thank the Biomedicum Functional Genomics Unit and the Biomedicum Clinical Proteomics unit for skilled scientific advice. This work has been supported by the Folkhälsan Research Foundation, the Sigrid Jusélius Foundation, the Finnish Epilepsy Association, Finska Läkaresällskapet (the Medical Society of Finland), Medicinska Understödsföreningen Liv och Hälsa r.f. ("Life and Health Medical Fund"), and Swedish Research Council. A-E.L. is a HiLIFE Fellow at the University of Helsinki. M.Y. is supported by the Scandinavia-Japan Sasakawa Foundation, the Japan Eye Bank Association, the Astellas Foundation for Research on Metabolic Disorders, and the Japan Society for the Promotion of Science Overseas Research Fellowships. S.K. is supported by Jane and Aatos Erkko Foundation and Swedish Research Council. The computations in this work were performed on resources provided by SNIC through Uppsala Multidisciplinary Center for Advanced Computational Science (UPPMAX) under Project SNIC 2017/7-317.

Appendix A. Supplementary data

Supplementary data to this article can be found online at https://doi.org/10.1016/j.nbd.2021.105418.

References

Adams-Cioaba, M.A., et al., 2011. Structural basis for the recognition and cleavage of histone H3 by cathepsin L. Nat. Commun. 2, 197. https://doi.org/10.1038/ncomms1204.

Agostini, M., et al., 2016. Metabolic reprogramming during neuronal differentiation. Cell Death Differ. 23, 1502–1514. https://doi.org/10.1038/cdd.2016.36.

Alakurtti, K., et al., 2005. Loss of lysosomal association of cystatin B proteins representing progressive myoclonus epilepsy, EPM1, mutations. Eur. J. Hum. Genet. 13, 208–215.

Allis, C.D., et al., 1980. Proteolytic processing of histone H3 in chromatin: a physiologically regulated event in Tetrahymena micronuclei. Cell. 20, 55–64. https://doi.org/10.1016/0092-8674(80)90234-2.

Andresen, K., et al., 2013. Solution scattering and FRET studies on nucleosomes reveal DNA unwrapping effects of H3 and H4 tail removal. PLoS One 8, e78587. https://doi.org/10.1371/journal.pone.0078587.

Azad, G.K., et al., 2018. Modifying chromatin by histone tail clipping. J. Mol. Biol. 430, 3051–3067. https://doi.org/10.1016/j.jmb.2018.07.013.

Benjamini, Y., Hochberg, Y., 1995. Controlling the false discovery rate - a practical and powerful approach to multiple testing. J. R. Stat. Soc. Ser. B Stat Methodol. 57, 289–300. https://doi.org/10.1111/j.2517-6161.1995.tb02031.x.

Brännvall, K., et al., 2003. Cystatin B is expressed by neural stem cells and by differentiated neurons and astrocytes. Biochem. Biophys. Res. Commun. 308, 369–374.

Brunet, J.F., et al., 2004. Early acquisition of typical metabolic features upon differentiation of mouse neural stem cells into astrocytes. Glia. 46, 8–17. https://doi.org/10.1002/glia.10348.

Bulynko, Y.A., et al., 2006. Cathepsin L stabilizes the histone modification landscape on the Y chromosome and pericentromeric heterochromatin. Mol. Cell. Biol. 26, 4172–4184. https://doi.org/10.1128/MCB.00135-06.

Buzzi, A., et al., 2012. Loss of cortical GABA terminals in Unverricht-Lundborg disease. Neurobiol. Dis. 47, 216–224. https://doi.org/10.1016/j.nbd.2012.04.005.

Canafoglia, L., et al., 2012. Electroclinical presentation and genotype-phenotype relationships in patients with Unverricht-Lundborg disease carrying compound heterozygous CSTB point and indel mutations. Epilepsia. 53, 2120–2127. https://doi.org/10.1111/j.1528-1167.2012.03718.x.

Ceru, S., et al., 2010. Stefin B interacts with histones and cathepsin L in the nucleus. J. Biol. Chem. 285, 10078–10086. https://doi.org/10.1074/jbc.M109.034793.

Chen, J.F., et al., 2014. Microcephaly disease gene Wdr62 regulates mitotic progression of embryonic neural stem cells and brain size. Nat. Commun. 5, 3885. https://doi.org/10.1038/ncomms4885.

Ciccolini, F., Svendsen, C.N., 1998. Fibroblast growth factor 2 (FGF-2) promotes acquisition of epidermal growth factor (EGF) responsiveness in mouse striatal precursor cells: identification of neural precursors responding to both EGF and FGF-2. J. Neurosci. 18, 7869–7880.

Ciptasari, U., van Bokhoven, H., 2020. The phenomenal epigenome in neurodevelopmental disorders. Hum. Mol. Genet. 29, R42–R50. https://doi.org/10.1093/hmg/ddaa175.
Dhaenens, M., et al., 2015. Histone proteolysis: a proposal for categorization into 'clipping' and 'degradation'. Bioessays. 37, 70–79. https://doi.org/10.1002/bies.201400118.
Di Matteo, F., et al., 2020. Cystatin B is essential for proliferation and interneuron migration in individuals with EPM1 epilepsy. EMBO Mol. Med. 12, e11419 https://doi.org/10.15252/emmm.201911419.
Duarte, L.F., et al., 2014. Histone H3.3 and its proteolytically processed form drive a cellular senescence programme. Nat. Commun. 5, 5210. https://doi.org/10.1038/ncomms6210.
Duncan, E.M., et al., 2008. Cathepsin L proteolytically processes histone H3 during mouse embryonic stem cell differentiation. Cell. 135, 284–294. https://doi.org/10.1016/j.cell.2008.09.055.
Felbor, U., et al., 2002. Neuronal loss and brain atrophy in mice lacking cathepsins B and L. Proc. Natl. Acad. Sci. U. S. A. 99, 7883–7888. https://doi.org/10.1073/pnas.112632299.
Francis, F., et al., 1999. Doublecortin is a developmentally regulated, microtubule-associated protein expressed in migrating and differentiating neurons. Neuron. 23, 247–256. https://doi.org/10.1016/s0896-6273(00)80777-1.
Gerdes, J., et al., 1983. Production of a mouse monoclonal antibody reactive with a human nuclear antigen associated with cell proliferation. Int. J. Cancer 31, 13–20. https://doi.org/10.1002/ijc.2910310104.
Gorski, K., et al., 2020. Quantitative changes in the mitochondrial proteome of cerebellar synaptosomes from preclinical cystatin B-deficient mice. Front. Mol. Neurosci. 13. https://doi.org/10.3389/fnmol.2020.570640.
Goulet, B., et al., 2004. A cathepsin L isoform that is devoid of a signal peptide localizes to the nucleus in S phase and processes the CDP/Cux transcription factor. Mol. Cell 14, 207–219. https://doi.org/10.1016/S1097-2765(04)00209-6.
Halangk, W., et al., 2000. Role of cathepsin B in intracellular trypsinogen activation and the onset of acute pancreatitis. J. Clin. Invest. 106, 773–781. https://doi.org/10.1172/JCI9411.
Hamalisto, S., et al., 2020. Spatially and temporally defined lysosomal leakage facilitates mitotic chromosome segregation. Nat. Commun. 11, 229. https://doi.org/10.1038/s41467-019-14009-0.
Herrera-Solorio, A.M., et al., 2019. Clipped histone H3 is integrated into nucleosomes of DNA replication genes in the human malaria parasite *Plasmodium falciparum*. EMBO Rep. 20 https://doi.org/10.15252/embr.201846331.
Islam, S., et al., 2011. Characterization of the single-cell transcriptional landscape by highly multiplex RNA-seq. Genome Res. 21, 1160–1167. https://doi.org/10.1101/gr.110882.110.
Islam, S., et al., 2014. Quantitative single-cell RNA-seq with unique molecular identifiers. Nat. Methods 11, 163–166. https://doi.org/10.1038/nmeth.2772.
Iwasaki, W., et al., 2018. Contribution of histone N-terminal tails to the structure and stability of nucleosomes (vol 3, pg 363, 2013). Febs Open Bio. 8, 1567. https://doi.org/10.1002/2211-5463.12508.
Iwata, R., et al., 2020. Mitochondrial dynamics in postmitotic cells regulate neurogenesis. Science. 369, 858–862. https://doi.org/10.1126/science.aba9760.
Jackson, C.B., et al., 2014. Mutations in SDHD lead to autosomal recessive encephalomyopathy and isolated mitochondrial complex II deficiency. J. Med. Genet. 51, 170–175. https://doi.org/10.1136/jmedgenet-2013-101932.
Joensuu, T., et al., 2007. Cystatin B: mutation detection, alternative splicing and expression in progressive myclonus epilepsy of Unverricht-Lundborg type (EPM1) patients. Eur. J. Hum. Genet. 15, 185–193. https://doi.org/10.1038/sj.ejhg.5201723.
Joensuu, T., et al., 2014. Gene expression alterations in the cerebellum and granule neurons of *Cstb*$^{-/-}$ mouse are associated with early synaptic changes and inflammation. PLoS One 9, e89321. https://doi.org/10.1371/journal.pone.0089321.
Khalkhali-Ellis, Z., et al., 2014. Cleavage of histone 3 by Cathepsin D in the involuting mammary gland. PLoS One 9, e103230. https://doi.org/10.1371/journal.pone.0103230.
Kim, D., et al., 2019. Graph-based genome alignment and genotyping with HISAT2 and HISAT-genotype. Nat. Biotechnol. 37, 907–915. https://doi.org/10.1038/s41587-019-0201-4.
Kim, K., et al., 2016. MMP-9 facilitates selective proteolysis of the histone H3 tail at genes necessary for proficient osteoclastogenesis. Genes Dev. 30, 208–219. https://doi.org/10.1101/gad.268714.115.
Koskenkorva, P., et al., 2011. Severer phenotype in Unverricht-Lundborg disease (EPM1) patients compound heterozygous for the dodecamer repeat expansion and the c.202C>T mutation in the CSTB gene. Neurodegener. Dis. 8, 515–522. https://doi.org/10.1159/000323470.
Lalioti, M.D., et al., 1997. Dodecamer repeat expansion in cystatin B gene in progressive myoclonus epilepsy. Nature. 386, 847–851. https://doi.org/10.1038/386847a0.
Lehesjoki, A.E., Kalviainen, R., 1993. Progressive myoclonic epilepsy type 1. In: Adam, M.P., et al. (Eds.), GeneReviews((R)), Seattle (WA).
Lehtinen, M.K., et al., 2009. Cystatin B deficiency sensitizes neurons to oxidative stress in progressive myoclonus epilepsy, EPM1. J. Neurosci. 29, 5910–5915. https://doi.org/10.1523/JNEUROSCI.0682-09.2009.
Lewis, E.M., Kroll, K.L., 2018. Development and disease in a dish: the epigenetics of neurodevelopmental disorders. Epigenomics. 10, 219–231. https://doi.org/10.2217/epi-2017-0113.
Liao, Y., et al., 2014. featureCounts: an efficient general purpose program for assigning sequence reads to genomic features. Bioinformatics. 30, 923–930. https://doi.org/10.1093/bioinformatics/btt656.
Love, M.I., et al., 2014. Moderated estimation of fold change and dispersion for RNA-seq data with DESeq2. Genome Biol. 15, 550. https://doi.org/10.1186/s13059-014-0550-8.
Maher, K., et al., 2014. A role for stefin B (cystatin B) in inflammation and endotoxemia. J. Biol. Chem. 289, 31736–31750. https://doi.org/10.1074/jbc.M114.609396.
Mancini, G.M., et al., 2016. CSTB null mutation associated with microcephaly, early developmental delay, and severe dyskinesia. Neurology. 86, 877–878. https://doi.org/10.1212/WNL.0000000000002422.
Manninen, O., et al., 2013. White matter degeneration with Unverricht-Lundborg progressive myoclonus epilepsy: a translational diffusion-tensor imaging study in patients and cystatin B-deficient mice. Radiology. 269, 232–239. https://doi.org/10.1148/radiol.13122458.
Manninen, O., et al., 2014. Progressive volume loss and white matter degeneration in CSTB-deficient mice: a diffusion tensor and longitudinal volumetry MRI study. PLoS One 9, e90709. https://doi.org/10.1371/journal.pone.0090709.
Melo, F.R., et al., 2017. Tryptase-catalyzed core histone truncation: a novel epigenetic regulatory mechanism in mast cells. J. Allergy Clin. Immunol. 140, 474–485. https://doi.org/10.1016/j.jaci.2016.11.044.
Montaser, M., et al., 2002. CA-074, but not its methyl ester CA-074Me, is a selective inhibitor of cathepsin B within living cells. Biol. Chem. 383, 1305–1308. https://doi.org/10.1515/BC.2002.147.
Morin, V., et al., 2012. The protease degrading sperm histones post-fertilization in sea urchin eggs is a nuclear cathepsin L that is further required for embryo development. PLoS One 7, e46850. https://doi.org/10.1371/journal.pone.0046850.
Nakagawa, T., et al., 1998. Cathepsin L: critical role in ii degradation and CD4 T cell selection in the thymus. Science. 280, 450–453. https://doi.org/10.1126/science.280.5362.450.
Nurse, N.P., et al., 2013. Clipping of flexible tails of histones H3 and H4 affects the structure and dynamics of the nucleosome. Biophys. J. 104, 1081–1088. https://doi.org/10.1016/j.bpj.2013.01.019.
O'Brien, A., et al., 2017. Severe neurodegeneration, progressive cerebral volume loss and diffuse hypomyelination associated with a homozygous frameshift mutation in CSTB. Eur. J. Hum. Genet. 25, 775–778. https://doi.org/10.1038/ejhg.2017.39.
Okuneva, O., et al., 2015. Abnormal microglial activation in the *Cstb*$^{-/-}$ mouse, a model for progressive myoclonus epilepsy, EPM1. Glia. 63, 400–411. https://doi.org/10.1002/glia.22760.
Penna, E., et al., 2019. Cystatin B involvement in synapse physiology of rodent brains and human cerebral organoids. Front. Mol. Neurosci. 12, 195. https://doi.org/10.3389/fnmol.2019.00195.
Pennacchio, L.A., et al., 1996. Mutations in the gene encoding cystatin B in progressive myoclonus epilepsy (EPM1). Science. 271, 1731–1734.
Pennacchio, L.A., et al., 1998. Progressive ataxia, myoclonic epilepsy and cerebellar apoptosis in cystatin B-deficient mice. Nat. Genet. 20, 251–258.
Pulvers, J.N., et al., 2010. Mutations in mouse Aspm (abnormal spindle-like microcephaly associated) cause not only microcephaly but also major defects in the germline. Proc. Natl. Acad. Sci. U. S. A. 107, 16595–16600. https://doi.org/10.1073/pnas.1010494107.
Rawlings, N.D., Barrett, A.J., 1990. Evolution of proteins of the cystatin superfamily. J. Mol. Evol. 30, 60–71.
Riccio, M., et al., 2001. Nuclear localization of cystatin B, the cathepsin inhibitor implicated in myoclonus epilepsy (EPM1). Exp. Cell Res. 262, 84–94.
Santos-Rosa, H., et al., 2009. Histone H3 tail clipping regulates gene expression. Nat. Struct. Mol. Biol. 16, 17–22. https://doi.org/10.1038/nsmb.1534.
Sergent-Tanguy, S., et al., 2006. Long-lasting coexpression of nestin and glial fibrillary acidic protein in primary cultures of astroglial cells with a major participation of nestin^{+}/GFAP^{-} cells in cell proliferation. J. Neurosci. Res. 83, 1515–1524. https://doi.org/10.1002/jnr.20846.
Shannon, P., et al., 2002. Neuropathological changes in a mouse model of progressive myoclonus epilepsy: cystatin B deficiency and Unverricht-Lundborg disease. J. Neuropathol. Exp. Neurol. 61, 1085–1091. https://doi.org/10.1093/jnen/61.12.1085.
Silva, A., et al., 2009. BDNF and extracellular matrix regulate differentiation of mice neurosphere-derived cells into a GABAergic neuronal phenotype. J. Neurosci. Res. 87, 1986–1996. https://doi.org/10.1002/jnr.22041.
Sommer, I., Schachner, M., 1981. Monoclonal antibodies (O1 to O4) to oligodendrocyte cell surfaces: an immunocytological study in the central nervous system. Dev. Biol. 83, 311–327. https://doi.org/10.1016/0012-1606(81)90477-2.
Styr, B., et al., 2019. Mitochondrial regulation of the hippocampal firing rate set point and seizure susceptibility. Neuron. 102, 1009–1024e8. https://doi.org/10.1016/j.neuron.2019.03.045.
Sun, Y., et al., 2008. Long-term tripotent differentiation capacity of human neural stem (NS) cells in adherent culture. Mol. Cell. Neurosci. 38, 245–258. https://doi.org/10.1016/j.mcn.2008.02.014.
Suslov, O.N., et al., 2002. Neural stem cell heterogeneity demonstrated by molecular phenotyping of clonal neurospheres. Proc. Natl. Acad. Sci. U. S. A. 99, 14506–14511. https://doi.org/10.1073/pnas.212525299.
Tegelberg, S., et al., 2012. Early microglial activation precedes neuronal loss in the brain of the Cstb−/− mouse model of progressive myoclonus epilepsy, EPM1. J. Neuropathol. Exp. Neurol. 71, 40–53. https://doi.org/10.1097/NEN.0b013e31823e68e1.
Torrado, E.F., et al., 2014. Directing mouse embryonic neurosphere differentiation toward an enriched neuronal population. Int. J. Dev. Neurosci. 37, 94–99. https://doi.org/10.1016/j.ijdevneu.2014.07.001.
Trimborn, M., et al., 2010. Establishment of a mouse model with misregulated chromosome condensation due to defective Mcph1 function. PLoS One 5, e9242. https://doi.org/10.1371/journal.pone.0009242.

Turk, V., Bode, W., 1991. The cystatins: protein inhibitors of cysteine proteinases. FEBS Lett. 285, 213–219. https://doi.org/10.1016/0014-5793(91)80804-c.
Uittenbogaard, M., et al., 2018. Epigenetic modifiers promote mitochondrial biogenesis and oxidative metabolism leading to enhanced differentiation of neuroprogenitor cells. Cell Death Dis. 9, 360. https://doi.org/10.1038/s41419-018-0396-1.
Vossaert, L., et al., 2014. Identification of histone H3 clipping activity in human embryonic stem cells. Stem Cell Res. 13, 123–134. https://doi.org/10.1016/j.scr.2014.05.002.
Yi, S.J., Kim, K., 2018. Histone tail cleavage as a novel epigenetic regulatory mechanism for gene expression. BMB Rep. 51, 211–218. https://doi.org/10.5483/bmbrep.2018.51.5.053.
Zheng, X., et al., 2016. Metabolic reprogramming during neuronal differentiation from aerobic glycolysis to neuronal oxidative phosphorylation. Elife. 5 https://doi.org/10.7554/eLife.13374.